Materials Today Chemistry 35 (2024) 101858

Contents lists available at ScienceDirect

Materials Today Chemistry

journal homepage: www.journals.elsevier.com/materials-today-chemistry/

Highly selective cathodic H_2O_2 electrosynthesis by a metal tellurate/carbon black composite material

Gabriel Alemany-Molina [a], Javier Fernández-Catalá [a,b,*], Wei Cao [b], Emilia Morallón [c], Diego Cazorla-Amorós [a,**]

[a] Department of Inorganic Chemistry and Materials Institute, University of Alicante, Ap. 99, Alicante, E-03080, Spain
[b] Nano and Molecular Systems Research Unit, University of Oulu, FIN-90014, Finland
[c] Department of Physical Chemistry and Materials Institute, University of Alicante, Ap. 99, Alicante, E-03080, Spain

A B S T R A C T

One sustainable alternative to the traditional anthraquinone technology to produce H_2O_2 is direct H_2O_2 electrosynthesis by oxygen reduction reaction (ORR). However, selecting electrocatalysts is a great challenge since most of the materials present selectivity towards the formation of H_2O (4-electron pathway). In this work, we present a facile electrocatalyst preparation consisting of Ni_3TeO_6 (NTO), a metal tellurate, mixed with carbon black (Vulcan) with outstanding selectivity (2.2 transferred electrons) towards the production of H_2O_2 by ORR. To test the possible real application, the NTO/Vulcan catalyst was tested in a long-term stability test showing excellent faradaic efficiency and 93.5 % of the initial current. TEM and XPS measurements after reaction show that NTO/Vulcan materials are robust and durable electrocatalysts. This work opens the door of novel materials such as metal tellurates based on Ni for their application as ORR electrocatalysts in industrial applications.

1. Introduction

Hydrogen peroxide (H_2O_2) has been used as clean oxidant used in many companies such as paper and pulp bleaching, synthesis of organic products, wastewater treatment or mining, among others [1–5]. The anthraquinone/hydroquinone process accounts for most of the H_2O_2 production today. However, there are exist several important drawbacks as the degradation of anthraquinone molecules, the huge use of organic solvents, and the use of stabilisers [6]. Furthermore, anthraquinone process is a batch method and requires a centralised production. The subsequent transportation of H_2O_2 rises its price and involves serious risks [6,7].

Electrochemical synthesis has been proposed as a green and on-site method for H_2O_2 decentralised production but materials with high activity, stability and cost-effective are required [6,8,9]. An alternative that has less aggressive potential conditions than in anodic production is cathodic production by oxygen reduction reaction (ORR). However, selecting electrocatalysts is difficult because most of the materials present mixed selectivity towards the formation of H_2O_2 (2-electron pathway) and H_2O (4-electron pathway) [9]. It has been observed that metal-based catalysts exhibit higher activity under alkaline solutions but higher selectivity towards the 2-electron path is reached in acidic media [9]. In basic media, low-cost materials based on earth abundant metals oxides are interesting for this application, but higher selectivity and durability is required [8,9]. The H_2O_2 produced in alkaline media, among other important applications, might be potentially used for lignocellulosic biomass pretreatment for biomass residues revalorization.

Transition metal tellurates such as M_3TeO_6 (MTO), which are composed by a 3d transition metal (M), such as Ni, Cu, Co …, tellurium (Te) and oxygen (O), exhibit several interesting properties for their future applications [10,11]. Most of the reported results of MTO have focused on study the magnetic properties due to the presence of transition metals (M = Ni, Co, Mn, Cu in MTO) in their structure with magnetic properties [11–13]. The optical and electronic properties and the presence of possible active sites (Transition metals) of metal tellurates open the door of this family of materials for their application in electrochemistry and catalysis [14–16]. One of the most promising and studied metal tellurates is Ni_3TeO_6 (NTO), after Newnham et al. investigated for the first time in 1967 the NTO crystal structure [17]. This material has a corundum type structure with a non-centrosymmetric space group R3, as was reported previously by scientific community [17,18]. A recent study further showed its existence in the 2D form with distinct photocatalytic properties over commonly seen pristine 2D peers

* Corresponding author.
** Corresponding author.
E-mail addresses: j.fernandezcatala@ua.es (J. Fernández-Catalá), cazorla@ua.es (D. Cazorla-Amorós).

https://doi.org/10.1016/j.mtchem.2023.101858
Received 3 October 2023; Received in revised form 28 November 2023; Accepted 11 December 2023
Available online 20 December 2023

[19]. Similarly, Cu_3TeO_6 (CTO) material is interesting for the scientific community due to the remarkable properties of copper in these systems [20,21]. The CTO crystal structure was first determined by Hostachy et al. [22] and revised in 1978 [23]. This material has a cubic structure (Ia3), as was described by Hostachy et al. [23]. In the last decades, the scientific community has focused on developing nickel and copper metal tellurates for their use in different applications such as electrocatalysis [24,25], photocatalysis [14] and sensors [26]. In this sense, our research group has developed NTO and CTO semiconductors using hydrothermal synthesis with interesting magnetic and photoconductivity properties, indicating that the synthesized NTO and CTO might be used in nanotechnologies such as photosensors [27]. However, to the best of our knowledge, it should be noted that, CTO or NTO have never been studied as electrocatalysts for ORR to produce H_2O_2, despite their roles in the aforementioned fields.

In this work, composite materials based on MTO and carbon black were prepared by a simple and reproducible synthetic protocol resulting in robust electrocatalysts. MTO were prepared by a green hydrothermal method and, after that, were physically mixed with carbon black to promote conductivity. Therefore, high temperatures or the use of organic solvents as DMF, that are required for the preparation of other electrocatalysts, were avoided and the scaling-up of the preparation of the electrocatalysts presented in this work would be very simple. Against the background of transition metals performing a limited selectivity towards the 2-electron pathway in basic media [9], we report a highly selective MTO electrocatalyst with excellent faradaic efficiency. Furthermore, as stability of the catalysts for H_2O_2 electrosynthesis is a critical issue, durability was studied and the used electrodes were analysed after a long-term potentiostatic experiment.

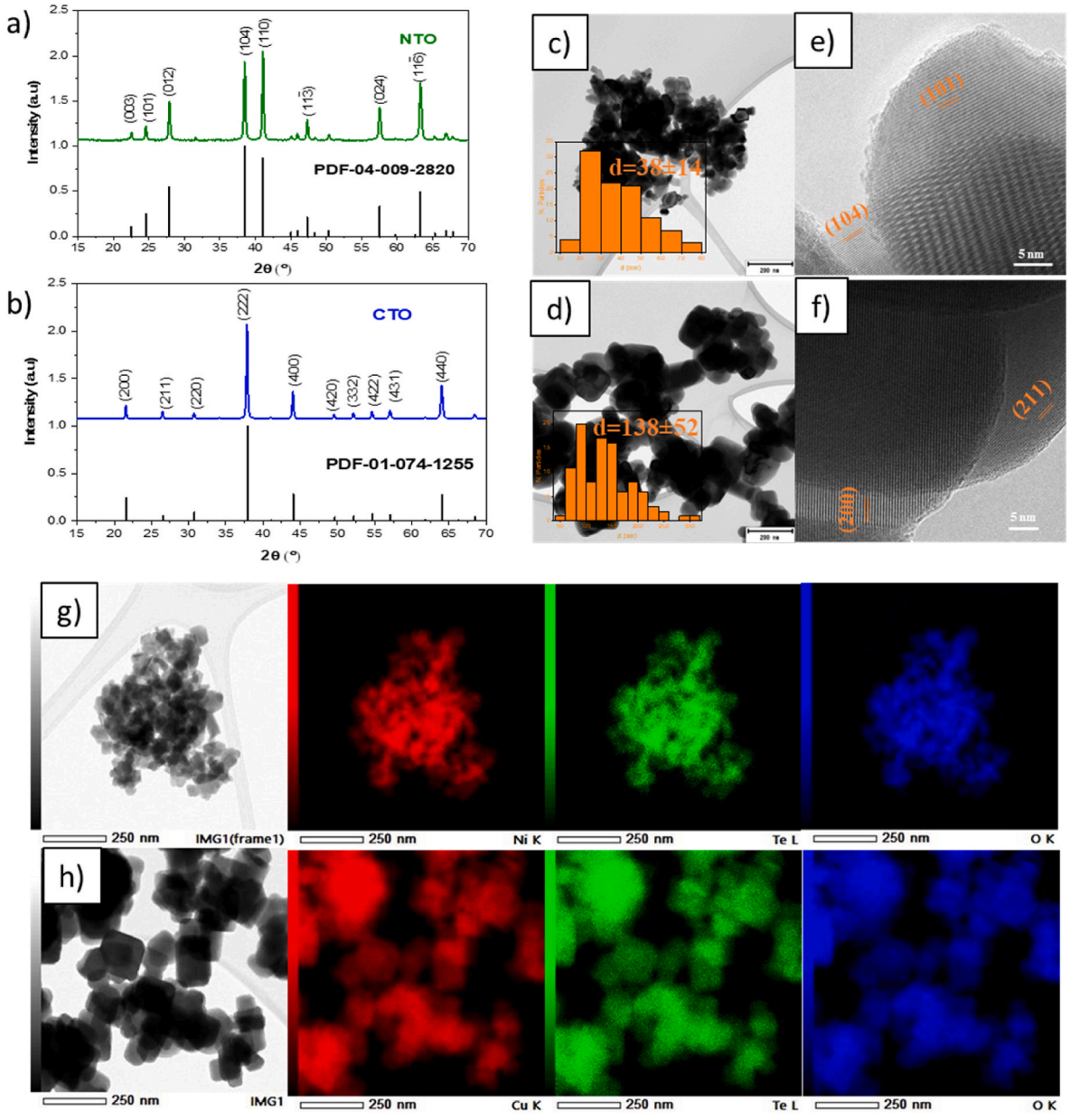

Fig. 1. (a) XRD patterns of the NTO and PDF-04-009-2828, (b) XRD patterns of the CTO and PDF-01-074-1255, (c) TEM image of NTO with histograms by counting 100 particles, (d) TEM image of CTO with histograms by counting 100 particles, (e) HR-TEM image of the NTO, (f) HR-TEM image of the CTO with histograms by counting 100 particles, (g) STEM images of NTO and elemental mapping images of Ni (red), Te (green), and O (blue) elements. (h) STEM images of CTO and elemental mapping images of Cu (red), Te (green), and O (blue) elements.

2. Materials and methods

NTO and CTO materials were prepared by hydrothermal synthesis, following the same synthesis methodology reported previously [27], see a detailed description of the synthetic procedures in SI "experimental section". The characterization and electrochemical characterization of the materials are described widely in the SI "experimental section". Also, the ORR condition tests are described in detail in SI "experimental section".

3. Results and discussion

3.1. Samples characterization

The structural and elemental analysis of the NTO and CTO materials, prepared following our previous synthesis and for their application in cathodic H_2O_2 production, by X-ray diffraction (XRD), transmission electron microscopy (TEM), and Scanning transmission electron microscopy coupled with Energy Dispersive X-ray Spectrometry analysis, were performed to proof that the materials were synthesized successfully.

The XRD results (Fig. 1 (a) and Fig. 1 (b)) show that the NTO and CTO phases are synthesized successfully since both materials present the corresponding diffraction peaks for Ni_3TeO_6 crystalline single phase (PDF 04-009-2820) [28] and Cu_3TeO_6 crystalline single phase (PDF 01-074-1255) in the experimental XRD diffractograms [26,29], as it was described previously [27]. TEM analysis (Fig. 1 (c,d)) show that NTO and CTO are synthesized forming nanoparticles (NPs) or particles, as it was previously reported [27]. Fig. 1 (c) shows that the Ni metal tellurate presents a heterogeneous morphology based on nanoparticles, with an average size of 38 nm, after counting 100 NPs. CTO sample also presents a heterogeneous morphology (Fig. 1 (d)) with an average size of 138 nm, after counting 100 particles. The metal tellurates show the high crystallinity as it is observed by HR-TEM images (Fig. 1 (d,f)). This fact also is verified by XRD analysis (Fig. 1 (a,b)). HR-TEM images of NTO (Fig. 1 (e)) presents d spacings of ~4.21 Å and 2.71 Å corresponding to the (101) and (104) crystalline planes for Ni_3TO_6 (PDF 04-009-2820), and the CTO sample presents d spacings of ~4.72 Å and 3.84 Å (Fig. 1 (f)), corresponding to the (200) and (211) planes for Cu_3TeO_6 crystalline phase (PDF 01-074-1255). STEM-EDS analysis was performed to study the elemental distribution of the NTO (Fig. 1 (g)) and CTO (Fig. 1 (h)) samples. Only presence of Ni or Cu (green), Te (blue), and O (red) elements homogeneously distributed in the sample NTO (Fig. 1 (g)) and CTO (Fig. 1 (h)) samples, was observed. The relative amount of the elements, as determined by EDS, M (Ni or Cu), Te, and O is very close to the stochiometric ratio (M_3TeO_6), indicating that each metal tellurate was synthesized successfully, as was reported previously in our research group. The results obtained by structural and elemental analysis are proof that the target tellurates (M_3TeO_6) have been successfully obtained using the hydrothermal methodology previously described [27].

3.2. Electrochemical characterisation

Fig. 2 (a,b) shows the cyclic voltammograms of the materials synthesized. Vulcan presented the typical voltammogram of a conductive carbon material. Bare NTO and NTO/Vulcan samples showed a voltammogram with a reversible peak centred at 0.74 V that may be related to $Ni(OH)_2$/NiOOH redox process in the surface [30]. NTO presents a very low current in the voltammogram and, for the composite samples (NTO/Vulcan_X), the double layer capacitance, measured between −0.1 V and 1.3 V, increases with the increase in the amount of carbon black (Table 1). On the other hand, CTO samples presented very different voltammograms. A Cu wire was measured for comparison purposes. The oxidation process observed in Cu between 0.75 and 1.2 V is related to the formation of $Cu(OH)_2$ and CuO; the minor processes centred in 0.55 V corresponds to CuO/Cu_2O redox process and the reduction reaction

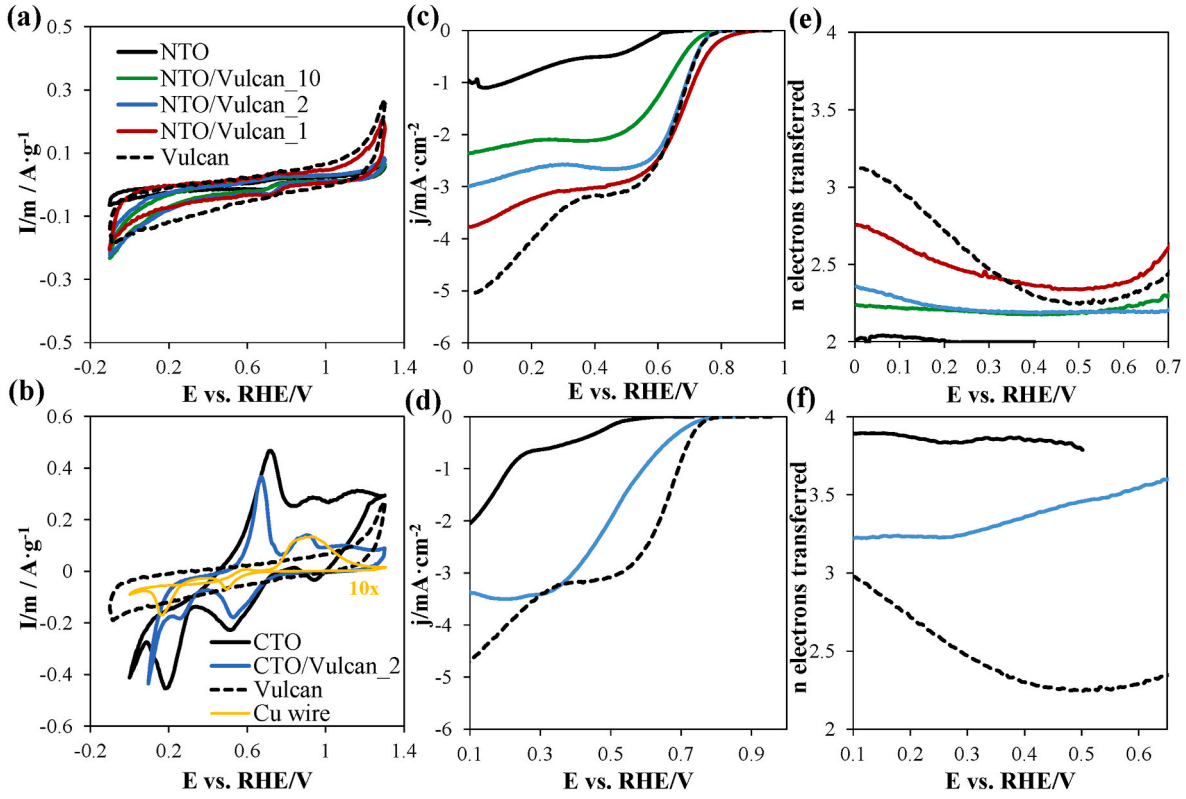

Fig. 2. Electrochemical characterization of metal tellurates for their use in ORR: (a–b) steady state voltammograms of the different samples at 5 mV s^{-1} (N_2-saturated), (c–d) LSV curves for the different samples and (e–f) number of electrons transferred,1600 rpm in a O_2-saturated 0.1 M KOH solution.

Table 1
Double layer capacitance (C), onset potential, half-wave potential ($E_{1/2}$), number of electrons transferred, H_2O_2 selectivity, limiting current density obtained from LSV curves for ORR, for the different catalysts.

Catalyst	C/F g^{-1}	E_{ONSET} /V	$E_{1/2}$ /V	N (E = 0.40 V)	H_2O_2 selectivity/% (E = 0.40V)	j/mA cm^{-2} (E = 0.40 V)
NTO	–	0.60	–	2.01	99	−0.51
NTO/Vulcan_1	7.4	0.79	0.68	2.50	75	−3.02
NTO/Vulcan_2	5.2	0.74	0.67	2.22	89	−2.64
NTO/Vulcan_10	4.7	0.72	0.62	2.07	96	−2.11
NiO/Vulcan_2	5.4	0.82	0.67	2.70	64	−3.05
CTO	–	0.56	–	3.85	8	−0.46
CTO/Vulcan	15.2	0.71	0.52	3.36	32	−2.94
Vulcan	12.0	0.75	0.66	2.30	85	−3.18

observed from 0.25 to 0.05 V is related to $Cu(OH)_2$ to Cu^0 [31]. The voltammogram obtained with CTO showed different profile than NTO with the appearance of different redox processes and indicating that these samples were more reactive than NTO even though the particle size of CTO was larger. Redox peaks presented similarities with Cu wire, but CuO/Cu_2O process was observed as the predominant peak. An oxidation and reduction process (centred at 1.15 and 0.95 V, respectively) was observed in CTO which can be related to Te-containing species [31,32]. This redox peak was not observed for NTO samples, indicating that Te may be highly stabilised in the NTO structure, although the Te element presents similar oxidation state in both samples, as was described in our previous report (Fig. S1) [27]. For CTO/-Vulcan_2 sample, the process is not clearly observed as consequence of the increase in the double layer current of carbon black, but the displacement towards higher potentials cannot ruled out. The reduction peak observed in the voltammograms and centred at around 0.2 V may also be the reduction process of $Cu(OH)_2$ to Cu^0. At more negative potentials, a high irreversible current starting at 0.05 and 0.15 V for CTO and CTO/Vulcan_2, respectively was observed. In Fig. S2 (a) it is shown the electrochemical behaviour at more negative potentials of CTO. At potentials lower than 0.1 V, a reduction peak is observed at around −0.34V that can be associated to the dissolution of the catalyst during the first cycle. For the subsequent cycles, the peak decreases and practically disappears in the third cycle. To analyze the nature of this reduction peak, XPS after cycling at more negative potentials (Fig. S2 (b)) was performed. The XPS showed that the satellite peak corresponding to Cu^{2+} decreased. This result indicates that the copper present in the CTO sample was reduced from Cu^{2+} to Cu^+ or Cu^0 [33,34]. Consequently, CTO materials at potentials lower than 0.1V in alkaline medium are unstable and are probably degraded, indicating that CTO is not suitable for ORR application.

ORR activity was evaluated in a 0.1 M KOH solution. LSV curves and the number of electrons transferred for the different MTO and Vulcan are shown in Fig. 2(c–f) and the information obtained from them is summarised in Table 1. The carbon black studied (Vulcan) presented relatively high selectivity for the H_2O_2 formation at low overpotentials. However, the selectivity was observed to decrease with the increasing overpotential until less than 50 % (Fig. 2 (c)). Far from it, bare NTO presented an exceptional selectivity towards the production of H_2O_2 (99 % selectivity at 0.4 V) where, even at high overpotentials, almost 100 % of the current was produced through a 2-electron pathway. However, the low conductivity of the NTO caused a very low current for the ORR (Fig. 2 (c)) [27]. At pH = 13, the thermodynamic potential of H_2O_2/O_2 is 0.74 vs. RHE [6]. The higher E_{ONSET} potential for NTO/Vulcan samples was observed in NTO/Vulcan_1 (0.79 V). For this sample, a synergistic effect is observed towards the 4-electron pathway as the number of electrons transferred is higher than that of Vulcan or NTO and E_{ONSET} potential was higher than the thermodynamic for H_2O_2 formation. At high overpotentials, mixed selectivity was observed (Fig. 2 (e)) because of the presence of carbon sites from Vulcan. NTO/Vulcan_2 sample presented negligible overpotential for H_2O_2 formation and the selectivity is shifted towards the 2-electron pathway. Contrary to what was observed for NTO/Vulcan_1 sample, the selectivity was maintained even at high overpotentials. Despite the higher amount of NTO, NTO/-Vulcan_10 sample presented a selectivity similar to NTO/Vulcan_2 but, due to the lower conductivity, the current reached for this sample was lower (Fig. 2 (c) and Table 1). Therefore, the optimal ratio for these samples was NTO/Vulcan_2 because appropriate conductivity was reached introducing the lower amount of carbon sites and therefore maintaining the outstanding selectivity of NTO.

EIS was also measured for NTO/Vulcan samples and experiments are shown in Fig. S3. For pure NTO, it can be observed that at 0.4 V the ORR is limited by charge transfer because of the poor electrical conductivity of the material. For the carbon black, at high frequencies, a Warburg resistance can be observed, which agrees with the diffusion of species that usually takes place in carbon materials. Finally, for NTO/Vulcan_2 electrocatalyst, because of the contact of NTO with a conductive material, the spectrum obtained corresponds to a behaviour of low impedance for the whole material.

CTO performance for ORR is shown in Fig. 2 (d,f). Similarly to NTO, the current density reached by bare CTO is low as expected for a semiconductor material, but presented high selectivity towards the 4-electron pathway (3.85 transferred electrons at 0.4 V). The performance observed for CTO is similar to that reported for CuO in basic media [35]. Considering the poor stability of CTO at low potentials, it is possible that CTO partially decomposes forming CuO. Thus, it cannot be discarded that part of the catalytic activity measured is related to the contribution from CuO sites. CTO/Vulcan_2 presented low E_{ONSET} potential, and the selectivity observed was a result of the combination of CTO and Vulcan sites, resulting in a non-selective electrocatalyst (Fig. 2 (f)). The poor electron transfer at low overpotentials may be associated to the higher particle size of CTO compared to NTO (~138 and ~38 nm, respectively). Furthermore, when applying low potentials, CTO-based samples decomposed. Therefore, while NTO presented high potential window and excellent selectivity, CTO-based materials cannot be considered as electrocatalysts for the ORR.

In order to deepen into the origin of the outstanding selectivity of NTO, a sample based on NiO (NiO/Vulcan_2) was studied to unravel the role of Te. Fig. 3 shows the comparison of the performance of NTO/Vulcan_2 and NiO/Vulcan_2 samples. NiO/Vulcan_2 sample showed mixed selectivity (2.70 of electron transfer number at 0.4 V) in comparison with NTO. The current density, the $E_{1/2}$ and the E_{ONSET} were higher for NiO/Vulcan_2 sample because of the H_2O formation. Therefore, with this test we demonstrate that, to reach the outstanding selectivity observed for NTO samples, materials based on NiO might not be enough and Te must be playing a key role. The effect of Te might be explained due to the metalloid properties of the tellurium as it was reported previously in literature using metalloid materials [36,37]. The particle size of the commercial NiO used (<50 nm) was similar to the prepared NTO, so other effects as the different Ni coordination may be considered. Ni coordinated with Te might produce different adsorption of O_2 and an optimal desorption of the OOH intermediate [38] in comparison with NiO/Vulcan sample. Also, additional effects due to the hydroxyl groups present on the NTO surface [19,26], compared to

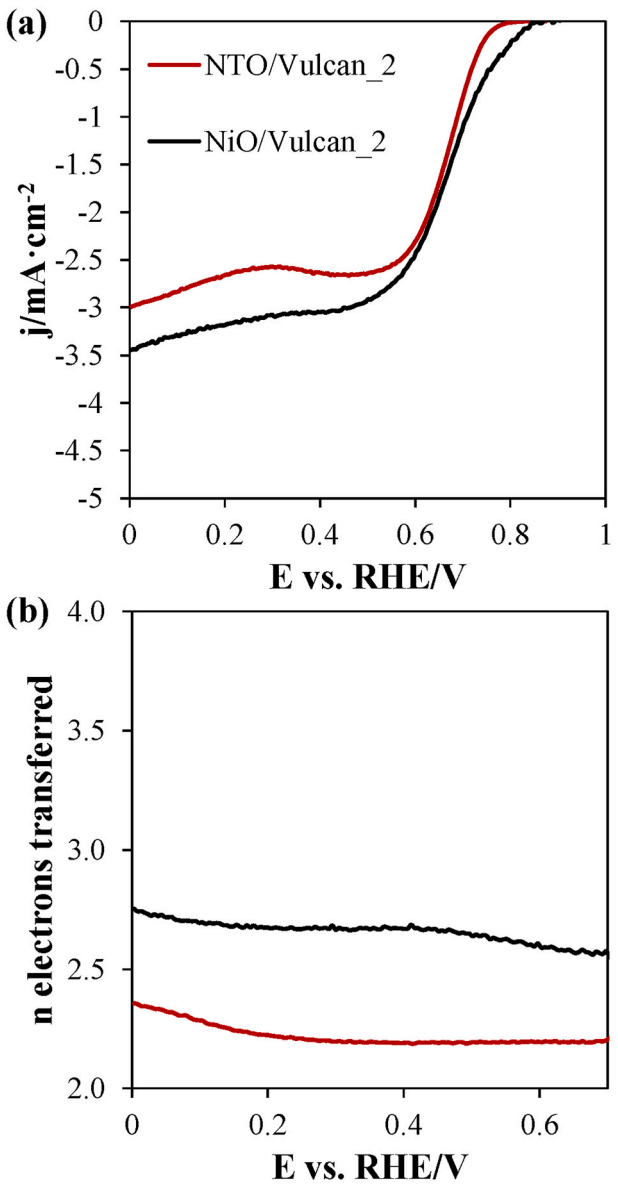

Fig. 3. Comparison between NTO and NiO for H_2O_2 electrosynthesis (a) LSV curves at 5 mV s^{-1} and (b) number of electrons transferred, 1600 rpm in a O_2-saturated 0.1 M KOH solution for NTO/Vulcan_2 compared to NiO/Vulcan_2.

commercial NiO analysed, cannot be discarded.

Fig. 4 presents the faradaic efficiency obtained in the stability test during 6 h at 0.4 V for the best sample (NTO/Vulcan_2). The electrocatalyst performed an excellent stability with a 93.5 % of the initial current maintenance after 6 h of reaction. The faradaic efficiency was measured to be over 90 % during the whole experiment, reaching a maximum value of 93 % in the first 2 h. These values are coherent with the number of electrons transferred at this potential (E = 0.4 V) measured with the RRDE. Faradaic efficiency over 90 % to produce H_2O_2 is remarkable in comparison with the values usually obtained with anodic H_2O_2 production and the excellent durability points metal tellurates as a promising robust electrocatalyst for cathodic H_2O_2 production in basic media. The concentration of H_2O_2 ($[H_2O_2]$) obtained after the stability test was 210 ppm (Fig. 4 (a)). Although low concentrations are required for water treatment (<0.1 wt %) [39], the H_2O_2 weight percentage could be widely improved by reducing the amount of electrolyte using a fuel cell configuration.

To further analyze the stability of the materials after reaction, the samples before and after reaction were studied by TEM and XPS. Fig. 5

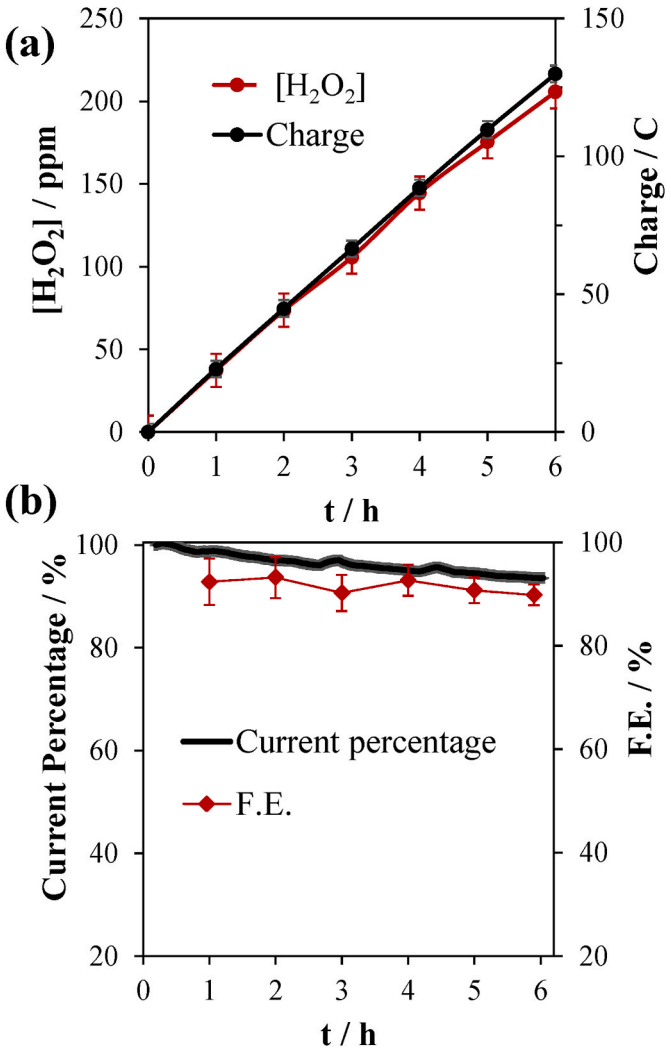

Fig. 4. Stability test for H_2O_2 production: (a) $[H_2O_2]$ and total charge, (b) faradaic efficiency in a O_2-saturated 1 M KOH solution for 6 h stability of NTO/Vulcan_2 sample (6h at 0.4V vs. RHE).

(a) shows that the spent samples did not experience any relevant changes with respect to the fresh samples by TEM analyses. This fact was also corroborated by counting 100 NPs of the NTO/Vulcan fresh (42 ± 15 nm) and used (39 ± 13 nm) sample indicating that there is not a significant change in the size of the fresh and after reaction NPs. XPS spectra of NTO/Vulcan_2 for Ni 2p signal before and after reaction showed that the sample was stable after stability test as no significant shift in the binding energy corresponding to Ni^{2+} of the bulk or $Ni(OH)_2$ on the surface of NTO was observed before and after the stability test (Fig. 5 (b)). Therefore, the high durability of the material during the chronoamperometric test is associated to the high stability of the composite material as shown in XPS and TEM experiments.

Several materials based on transition metals have been studied before for cathodic H_2O_2 production in basic media [40–44]. Some examples are given in Table 2. Overall, the prepared NTO/Vulcan_2 sample can be considered as a promising material in terms of the excellent selectivity, which is comparable to the other electrocatalysts shown, and adequate E_{ONSET}. Moreover, faradaic efficiency is superior to some of the materials.

4. Conclusions

Cathodic production of hydrogen peroxide presents important

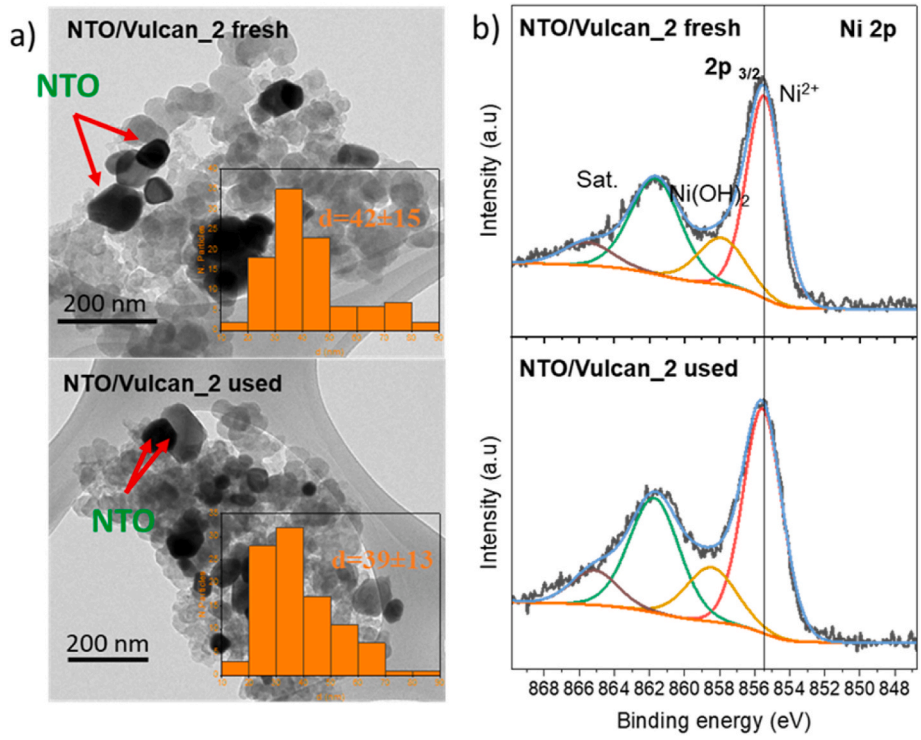

Fig. 5. Stability of the materials after reaction using TEM and XPS: (a) TEM image and (b) XPS spectra of NTO/Vulcan_2 Ni 2p signal before and after reaction.

Table 2
Comparison of performance for H_2O_2 cathodic electrosynthesis with other metal-based materials (O_2-saturated at 1600 rpm).

Catalyst	$E_{ONSET\ ORR}$/V	ntransferred electrons *(E=0.40 V)*	*FE/% (E=0.40 V)*	Electrolyte	Reference
NTO/Vulcan_2	0.74	2.2	93	0.1 M KOH	This work
Sb-NSCF	0.76	2.2	90	0.1 M KOH	[40]
c-Mo/NCPs	~0.8	2.4	82	0.1 M KOH	[41]
$Ni_{2-x}P$-V_{Ni}	0.78	2.1	83.6	0.1 M KOH	[42]
CoPc-OCNT	0.77	2.1	>95 %[a]	1 M KOH	[43]
CeO_2/C	0.84	2.1	–	1 M NaOH	[44]
Co_1@GO	0.91	2.3	–	0.1 M KOH	[45]

[a] Determined at j = −100 mA cm^{-2}.

challenges regarding the preparation of new cost-effective, durable, and highly selective electrocatalysts. From our knowledge, we have studied for the first time several composite materials, based on metal tellurates and carbon black that were prepared by a simple and easily scalable synthetic protocol, in H_2O_2 electrosynthesis.

The optimal ratio of carbon black for preparing the composite MTO/Vulcan materials was studied with the RRDE and it was observed that the best performance was obtained for NTO/Vulcan_2 material which contains a weight ratio of 2:1. For higher amounts of Vulcan, the outstanding selectivity towards the 2-electron path was not achieved and mixed selectivity was observed. The results obtained open the door to the use of NTO as electrocatalyst in H_2O_2 synthesis. CTO-based samples could not be considered as adequate electrocatalysts due to the instability observed at low potentials. NTO/Vulcan_2 material showed excellent faradaic efficiency and outstanding durability at constant potential as it maintained a 93.5 % of the initial current. This work also highlights the role of metalloid elements (Te) in the selective H_2O_2 production compared to nickel oxide semiconductors. Comparing the values obtained with other published metal-based electrocatalysts for cathodic H_2O_2 production, NTO/Vulcan composites stand out as promising materials due to the high selectivity reached and the simple and easy-scalable synthesis protocol. This work highlights, for the first time, the interest of the NTO/Vulcan materials synthesized using an easy methodology for their application in H_2O_2 electrosynthesis.

CRediT authorship contribution statement

Gabriel Alemany-Molina: Conceptualization, Investigation, Methodology, Writing - original draft. **Javier Fernández-Catalá:** Conceptualization, Investigation, Methodology, Writing - original draft, Writing - review & editing. **Wei Cao:** Conceptualization, Funding acquisition, Writing - review & editing. **Emilia Morallón:** Conceptualization, Funding acquisition, Methodology, Project administration, Supervision, Writing - review & editing. **Diego Cazorla-Amorós:** Conceptualization, Funding acquisition, Methodology, Project administration, Supervision, Writing - review & editing.

Declaration of competing interest

The authors declare that they have no known competing financial interests or personal relationships that could have appeared to influence the work reported in this paper.

Data availability

Data will be made available on request.

Acknowledgments

This work was support by PID2021-123079OB-I00 project funded by MCIN/AEI/10.13039/501100011033, "ERDF A way of making Europe" and the European Research Council (ERC) under the European Union's Horizon 2020 research and innovation programme (grant agreement no. 101002219). GAM thanks Ministerio de Universidades for the FPU20/03969 grant. JFC thanks MARSALAS21-09 contract funded by MCIN/AEI/10.13039/501100011033 and, European Union NextGenerationEU/PRTR.

Appendix A. Supplementary data

Supplementary data to this article can be found online at https://doi.org/10.1016/j.mtchem.2023.101858.

References

[1] R. Hage, A. Lienke, Applications of transition-metal catalysts to textile and wood-pulp bleaching, Angew. Chem., Int. Ed. 45 (2006), https://doi.org/10.1002/anie.200500525, 206–222.
[2] N. Agarwal, S.J. Freakley, R.U. Mcvicker, S.M. Althahban, N. Dimitratos, Q. He, D. J. Morgan, R.L. Jenkins, D.J. Willock, S.H. Taylor, C.J. Kiely, G.J. Hutchings, Aqueous Au-Pd colloids catalyze selective CH_4 oxidation to CH_3OH with O_2 under mild conditions, Science 358 (2017) 223–227, https://doi.org/10.1126/science.aan6515.
[3] E. Brillas, I. Sirés, M.A. Oturan, Electro-fenton process and related electrochemical technologies based on fenton's reaction Chemistry, Chem. Rev. 109 (2009) 6570–6631, https://doi.org/10.1021/cr900136g.
[4] Hydrogen Peroxide Market Size By End-User. https://www.Gminsights.Com/Industry-Analysis/Hydrogen-Peroxide-Market (Accessed April 27, 2023).
[5] B. Puértolas, A.K. Hill, T. García, B. Solsona, L. Torrente-Murciano, In-situ synthesis of hydrogen peroxide in tandem with selective oxidation reactions: a mini-review, Catal. Today 248 (2015) 115–127, https://doi.org/10.1016/j.cattod.2014.03.054.
[6] S. Yang, A. Verdaguer-Casadevall, L. Arnarson, L. Silvioli, V. Čolić, R. Frydendal, J. Rossmeisl, I. Chorkendorff, I.E.L. Stephens, Toward the decentralized electrochemical production of H_2O_2: a focus on the catalysis, ACS Catal. 8 (2018) 4064–4081, https://doi.org/10.1021/acscatal.8b00217.
[7] M25 Chaos after Lorry Explosion. http://news.bbc.co.uk/2/hi/uk_news/england/london/4197500.stm. (Accessed June 21, 2023)..
[8] Y. Tian, D. Deng, L. Xu, M. Li, H. Chen, Z. Wu, S. Zhang, Strategies for sustainable production of hydrogen peroxide via oxygen reduction reaction: from catalyst design to device setup, Nano-Micro Lett. 15 (2023) 122, https://doi.org/10.1007/s40820-023-01067-9.
[9] X. Huang, M. Song, J. Zhang, T. Shen, G. Luo, D. Wang, Recent advances of electrocatalyst and cell design for hydrogen peroxide production, Nano-Micro Lett. 15 (2023) 86, https://doi.org/10.1007/s40820-023-01044-2.
[10] Y.S. Oh, S. Artyukhin, J.J. Yang, V. Zapf, J.W. Kim, D. Vanderbilt, S.W. Cheong, Non-hysteretic colossal magnetoelectricity in a collinear antiferromagnet, Nat. Commun. 5 (2014) 1–7, https://doi.org/10.1038/ncomms4201.
[11] R. Mathieu, S.A. Ivanov, P. Nordblad, M. Weil, Enhancement of antiferromagnetic interaction and transition temperature in M_3TeO_6 systems (M = Mn, Co, Ni, Cu), Eur. Phys. J. B 86 (2013) 3–6, https://doi.org/10.1140/epjb/e2013-40152-x.
[12] M. Numan, G. Das, M.S. Khan, G. Manna, A. Banerjee, S. Giri, G. Aquilanti, S. Majumdar, Evidence of exchange striction and charge disproportionation in the magnetoelectric material Ni_3TeO_6, Phys. Rev. B 106 (2022), 214437, https://doi.org/10.1103/PhysRevB.106.214437.
[13] J.W. Kim, S. Artyukhin, E.D. Mun, M. Jaime, N. Harrison, A. Hansen, J.J. Yang, Y. S. Oh, D. Vanderbilt, V.S. Zapf, S.W. Cheong, Successive magnetic-field-induced transitions and colossal magnetoelectric effect in Ni_3TeO_6, Phys. Rev. Lett. 115 (2015) 1–5, https://doi.org/10.1103/PhysRevLett.115.137201.
[14] L. Xu, C. Qin, H. Xie, Y. Huang, L. Qin, H.J. Seo, Ilmenite-type semiconductor Ni_3TeO_6: preparation, optical property and photo-degradation ability, Mater. Lett. 184 (2016) 1–4, https://doi.org/10.1016/j.matlet.2016.08.008.
[15] A. Yamuna, N. Karikalan, T.Y. Lee, Effect of the Ni_3TeO_6 phase in a $Ni_2Te_3O_8$/expanded graphite composite on the electrochemical monitoring of metribuzin residue in soil and water samples, J. Hazard Mater. 435 (2022), 128988, https://doi.org/10.1016/j.jhazmat.2022.128988.
[16] S.D. Mardolkar, A.V. Salker, Insulator-semiconductor transitions and photo-luminescent behaviour in doped copper tellurates, Mater. Sci. Semicond. Process. 105 (2020), 104758, https://doi.org/10.1016/j.mssp.2019.104758.
[17] R.E. Newnham, E.P. Meagher, Structure of Ni_3TeO_6, Mater. Res. Bull. 2 (1967) 549–554.
[18] R. Becker, H. Berger, Reinvestigation of Ni_3TeO_6, Acta Crystallogr. Sect. E Struct. 62 (2006) 222–223, https://doi.org/10.1107/S1600536806043042.
[19] J. Fernández-Catalá, A.A. Kistanov, Y. Bai, H. Sing, W. Cao, Theoretical prediction and shape-controlled synthesis of two-dimensional semiconductive Ni_3TeO_6. npj 2D Mater, Appl 7 (2023) 48, https://doi.org/10.1038/s41699-023-00412-1.
[20] J. Chakraborty, Ab initio calculations on three dimensional antiferromagnet Cu_3TeO_6, J. Phys. Chem. Solid. 134 (2019) 182–186, https://doi.org/10.1016/j.jpcs.2019.05.038.
[21] S. Bao, Z. Cai, W. Si, W. Wang, X. Wang, Y. Shangguan, Z. Ma, Z.Y. Dong, R. Kajimoto, K. Ikeuchi, S.L. Yu, J. Sun, J.X. Li, J. Wen, Evidence for magnon-phonon coupling in the topological magnet Cu_3TeO_6, Phys. Rev. B 101 (2020), 214419, https://doi.org/10.1103/PhysRevB.101.214419.
[22] A. Hostachyand, J. Coing-Boyat, Structure crystalline de Cu_3TeO_6, C. R. Acad. Sci. 267 (1968) 1435.
[23] B.Y.L. Falck, O. Lindqvist, P.E. Bataillon, Tricopper(ll) Tellurate(Vl) 18 (1978) 896–897.
[24] M.Z. Iqbal, E. Carleschi, B.P. Doyle, R.J. Kriek, Photocharged water splitting employing a nickel(II) tellurium oxide (Photo)Anode in alkaline medium, ACS Appl. Energy Mater. 2 (2019) 8125–8137, https://doi.org/10.1021/acsaem.9b01597.
[25] S. Park, S. Park, V. Mathew, B. Sambandam, J.Y. Hwang, J. Kim, A new tellurium-based Ni_3TeO_6-carbon nanotubes composite anode for Na-ion battery, Int. J. Energy Res. 46 (2022) 16041–16049, https://doi.org/10.1002/er.8221.
[26] B. Mutharani, R. Rajakumaran, S.M. Chen, P. Ranganathan, T.W. Chen, D.A. Al Farraj, M.A. Ali, F.M.A. Al-Hemaid, Facile synthesis of 3D stone-like copper tellurate (Cu_3TeO_6) as a new platform for anti-inflammatory drug ibuprofen sensor in human blood serum and urine samples, Microchem. J. 159 (2020), 105378, https://doi.org/10.1016/j.microc.2020.105378.
[27] J. Fernández-Catalá, H. Singh, S. Wang, H. Huhtinen, P. Paturi, Y. Bai, W. Cao, Hydrothermal synthesis of Ni_3TeO_6 and Cu_3TeO_6 nanostructures for magnetic and photoconductivity applications, ACS Appl. Nano Mater. 6 (2023) 4887–4897, https://doi.org/10.1021/acsanm.3c00630.
[28] M. Numan, M.S. Khan, S. Majumdar, Vacancy induced mixed valence state in nickel tellurate Ni_3TeO_6, Mater. Today Proc. 57 (2022) 151–156, https://doi.org/10.1016/j.matpr.2022.02.202.
[29] S.D. Mardolkar, A.V. Salker, Efficiently synthesized Co doped Cu_3TeO_6 accounted for its anomalous behaviour in electronic properties, New J. Chem. 41 (2017) 13974–13982, https://doi.org/10.1039/c7nj02981k.
[30] H. Cheshideh, F. Nasirpouri, Cyclic voltammetry deposition of nickel nanoparticles on TiO_2 nanotubes and their enhanced properties for electro-oxidation of methanol, J. Electroanal. Chem. 797 (2017) 121–133, https://doi.org/10.1016/j.jelechem.2017.05.024.
[31] S.D. Giri, A. Sarkar, Electrochemical study of bulk and monolayer copper in alkaline solution, J. Electrochem. Soc. 163 (2016) 252–259, https://doi.org/10.1149/2.0071605jes.
[32] M.J.N. Pourbaix, Atlas of electrochemical equilibria in aqueous solutions, J. Electroanal. Chem. Interfacial Electrochem. (1974) 644.
[33] X. Xie, J. Liu, T. Li, Y. Song, F. Wang, Post-Formation copper-nitrogen species on carbon black: their chemical structures and active sites for oxygen reduction reaction, Chem. Eur J. 24 (2018) 9968–9975, https://doi.org/10.1002/chem.201801764.
[34] Q. He, X. Yang, X. Ren, B.E. Koel, N. Ramaswamy, S. Mukerjee, R. Kostecki, A novel CuFe-based catalyst for the oxygen reduction reaction in alkaline media, J. Power Sources 196 (2011) 7404–7410, https://doi.org/10.1016/j.jpowsour.2011.04.016.
[35] J. Yu, T. Huang, Z. Jiang, M. Sun, C. Tang, A hybrid mateiral combined copper oxide with graphene for an oxygen reduction reaction in an alkaline medium, Molecules 24 (2) (2019) 411, https://doi.org/10.3390/molecules24030441.
[36] F. Ma, S. Wang, X. Liang, C. Wang, F. Tong, Z. Wang, P. Wang, Y. Liu, Y. Dai, Z. Zheng, B. Huang, Ni_3B as a highly efficient and selective catalyst for the electrosynthesis of hydrogen peroxide, Appl. Catal., B 279 (2020), 11937, https://doi.org/10.1016/j.apcatb.2020.119371.
[37] K. Jiang, S. Back, A.J. Akey, C. Xia, Y. Hu, W. Liang, D. Schaak, E. Stavitski, J. K. Nørskov, S. Siahrostami, H. Wang, Highly selective oxygen reduction to hydrogen peroxide on transition metal single atom coordination, Nat. Commun. 10 (2019) 3997, https://doi.org/10.1038/s41467-019-11992-2.
[38] J.X. Flores-Lasluisa, F. Huerta, D. Cazorla-Amorós, E. Morallón, $LaNi_{1-x}Co_xO_3$ perovskites for application in electrochemical reactions involving molecular oxygen, Energy 273 (2023), 127256, https://doi.org/10.1016/j.energy.2023.127256.
[39] M.N. Young, M.J. Links, S.C. Popat, B.E. Rittmann, C.I. Torres, Tailoring microbial electrochemical cells for production of hydrogen peroxide at high concentrations and efficiencies, ChemSusChem 9 (2016) 3345–3352, https://doi.org/10.1002/cssc.201601182.
[40] M. Yan, Z. Wei, Z. Gong, B. Johannessen, G. Ye, G. He, J. Liu, S. Zhao, C. Cui, H. Fei, Sb_2S_3-Templated synthesis of sulfur-doped Sb-N-C with hierarchical architecture and high metal loading for H_2O_2 electrosynthesis, Nat. Commun. 14 (2023) 1–10, https://doi.org/10.1038/s41467-023-36078-y.
[41] M. Jin, S. Liu, G. Meng, S. Zhang, Q. Liu, J. Luo, X. Liu, Low-coordinated Mo clusters for high-efficiency electrocatalytic hydrogen peroxide production, Adv. Mater. Interfac. 10 (2023) 1–7, https://doi.org/10.1002/admi.202201144.
[42] Z. Zhou, Y. Kong, H. Tan, Q. Huang, C. Wang, Z. Pei, H. Wang, Y. Liu, Y. Wang, S. Li, X. Liao, W. Yan, S. Zhao, Cation-vacancy-enriched nickel phosphide for efficient electrosynthesis of hydrogen peroxides, Adv. Mater. 34 (2022), 2106541, https://doi.org/10.1002/adma.202106541.
[43] P. Cao, X. Quan, X. Nie, K. Zhao, Y. Liu, S. Chen, H. Yu, J.G. Chen, Metal single-site catalyst design for electrocatalytic production of hydrogen peroxide at industrial-relevant currents, Nat. Commun. 14 (2023) 1–12, https://doi.org/10.1038/s41467-023-35839-z.
[44] V.S. Pinheiro, E.C. Paz, L.R. Aveiro, L.S. Parreira, F.M. Souza, P.H.C. Camargo, M. C. Santos, Ceria high aspect ratio nanostructures supported on carbon for hydrogen peroxide electrogeneration, Electrochim. Acta 259 (2018) 865–872, https://doi.org/10.1016/j.electacta.2017.11.010.
[45] B. Zhang, T. Zheng, Y. Wang, Y. Du, S. Chu, Z. Xia, R. Amal, S. Dou, L. Dai, Highly efficient and selective electrocatalytic hydrogen peroxide production on Co-O-C

active centers on graphene oxide, Commun. Chem. 5 (2022) 43, https://doi.org/10.1038/s42004-022-00645-z.